Journal of Nuclear Medicine, published on June 4, 2021 as doi:10.2967/jnumed.121.262083

^{11}C-PIB and ^{124}I-antibody PET provide differing estimates of brain amyloid-beta after therapeutic intervention

Silvio R Meier[1], Dag Sehlin[1], Sahar Roshanbin[1], Victoria Lim Falk[1], Takashi Saito[2,3], Takaomi C Saido[2], Ulf Neumann[4], Johanna Rokka[1], Jonas Eriksson[5,6] and Stina Syvänen[1]

[1]Department of Public Health and Caring Sciences/Geriatrics, Uppsala University, Uppsala, Sweden
[2]Laboratory for Proteolytic Neuroscience, RIKEN Center for Brain Science, Wako, Saitama, 351-0198, Japan
[3]Department of Neurocognitive Science, Institute of Brain Science, Nagoya City University Graduate School of Medical Sciences, 1 Kawasumi, Mizuho-ku, Mizuho-cho, Nagoya, Aichi 467-8601, Japan
[4]Neuroscience Research, Novartis Institutes for BioMedical Research, Basel, Switzerland
[5]Department of Medicinal Chemistry, Uppsala Biomedical Center, Uppsala University, Uppsala, Sweden
[6]PET Centre, Uppsala University Hospital, Uppsala, Sweden

Article type: Original research

Running title ^{11}C-PIB vs ^{124}I-antibody PET

Corresponding Author: Stina Syvänen, Department of Public Health and Caring Sciences/Geriatrics, Uppsala University, Rudbecklaboratoriet, 751 85 Uppsala, Sweden; stina.syvanen@pubcare.uu.se; +4618-471 3405

First author: Silvio Meier, Department of Public Health and Caring Sciences/Geriatrics, Uppsala University, Rudbecklaboratoriet, 751 85 Uppsala, Sweden, silvio.meier@pubcare.uu.se, +4618-471 5038, PhD student

ABSTRACT

Positron emission tomography (PET) imaging of amyloid-β (Aβ) has become an important component of Alzheimer´s disease (AD) diagnosis. ^{11}C-Pittsburgh compound B (^{11}C-PiB) and analogs bind to fibrillar Aβ. However, levels of nonfibrillar, soluble aggregates of Aβ, appear more dynamic during disease progression and more affected by Aβ reducing treatments. The aim of this study was to compare an antibody-based PET ligand, targeting nonfibrillar Aβ, with ^{11}C-PiB after β-secretase (BACE-1) inhibition in two AD mouse models at an advanced stage of Aβ pathology.

Methods: Transgenic ArcSwe mice (16 months) were treated with the BACE-1 inhibitor NB-360 for 2 months, while another group was kept as controls. A third group was analyzed at the age of 16 months as baseline. Mice were PET scanned with ^{11}C-PiB to measure Aβ plaque load followed by a scan with the bispecific radioligand ^{124}I-RmAb158-scFv8D3 to investigate nonfibrillar aggregates of Aβ. The same study design was then applied for another mouse model, *App*$^{NL-G-F}$. In this case, NB-360 treatment was initiated at the age of 8 months and animals were scanned with ^{11}C-PiB-PET and ^{125}I-RmAb158-scFv8D3 single-photon emission computer tomography (SPECT). Brain tissue was isolated after scanning and Aβ levels were assessed.

Results: ^{124}I-RmAb158-scFv8D3 concentrations measured with PET in hippocampus and thalamus of NB-360 treated ArcSwe mice were similar to those observed in baseline animals and significantly lower than concentrations observed in same-age untreated controls. Reduced ^{125}I-RmAb158-scFv8D3 retention was also observed with SPECT in hippocampus, cortex and cerebellum of NB-360 treated *App*$^{NL-G-F}$ mice. Radioligand *in vivo* concentrations corresponded with postmortem brain tissue analysis of soluble Aβ aggregates. For both models, mice treated with NB-360 did not display a reduced ^{11}C-PiB signal compared to untreated controls, and further, both NB-360 and control mice tended, although not reaching significance, to show higher ^{11}C-PiB signal than the baseline groups.

Conclusion: This study demonstrated the ability of an antibody-based radioligand to detect changes in brain Aβ levels after anti-Aβ therapy in ArcSwe and *App*$^{NL-G-F}$ mice with pronounced Aβ pathology. In contrast, the decreased Aβ levels could not be quantified with ^{11}C-PiB PET, suggesting that these ligands detect different pools of the Aβ.

Key words: Alzheimer´s Disease, BACE-1 inhibition, Amyloid-beta, ^{11}C-PiB, Antibody-based PET

INTRODUCTION

Alzheimer´s disease (AD) is a growing socioeconomic burden on the society and health care that in most countries is characterized by an aging population (*1*). In spite of intense research over the last decades, no treatment is available that halts the underlying disease mechanisms and stops the pathological changes in the AD brain. Accumulation of amyloid-beta (Aβ) plaques is the core feature of histopathological diagnosis of AD and can be visualized and quantified by molecular imaging. Positron emission tomography (PET) is today a valuable tool for assessment of brain amyloidosis *in vivo*. Amyloid imaging with PET has also become a regularly used inclusion criterion for enrolment of patients in clinical trials. New treatments, aiming to clear Aβ from the brain parenchyma or to reduce Aβ production and aggregation, are dependent on diagnostic tools to follow changes in brain Aβ levels *in vivo*.

PET ligands such as ^{11}C-Pittsburgh compound B (^{11}C-PiB) and several later developed analogues bind to fibrillar Aβ, i.e. the form of Aβ found in insoluble amyloid plaques. However, Aβ aggregation starts years before any clinical symptoms emerge, and it appears as the PET signal with amyloid radioligands such as ^{11}C-PiB become saturated rather early during disease progression (*2, 3*). In contrast, nonfibrillar Aβ oligomers and protofibrils have been reported to display a more dynamic profile during the course of the clinical stages of the disease and may therefore be better biomarkers for disease severity than amyloid plaques (*3, 4*). Treatments aimed at reducing brain Aβ, such as BACE-1 inhibitors, or to facilitate Aβ clearance, e.g. immunotherapy, are likely to reduce nonfibrillar Aβ before amyloid plaques (*5, 6*). Furthermore, diffuse Aβ plaque pathology cannot be detected by these radioligands, which bind to the ordered β-sheet structures of amyloid plaques (*7*).

A potential strategy to image nonfibrillar Aβ aggregates, rather than plaques, and thus a way to circumvent the limitations of ^{11}C-PiB and other amyloid radioligands could be to use an antibody-based PET approach. Antibodies are characterized by high and specific binding to

their target, and can be generated to show selective affinity for a specific aggregation form of Aβ, e.g. Aβ protofibrils (*8*). However, antibodies display very limited passage across the blood-brain barrier and are therefore not directly suitable as radioligands that require fast and efficient brain entry. We have recently introduced several bispecific radioligands based on Aβ binding antibodies functionalized with a transferrin receptor (TfR) binding component to enable active transport across the blood-brain barrier (*9-13*).

RmAb158-scFv8D3 (*14*) is based on the Aβ protofibril selective antibody mAb158 (*8, 15*), the murine version of *Lecanemab* (*16*) that is currently evaluated as an anti-Aβ treatment in clinical phase III trials, and two single chain fragments (scFv) of the TfR antibody 8D3 (*17*), to enhance brain uptake. A previous study showed that PET with iodine-124 labelled RmAb158-scFv8D3 could be used to successfully follow Aβ accumulation in mice, 7 to 16 months of age, harboring the Arctic (Aβ precursor protein [APP] E693G) and the Swedish (APP KM670/671NL) APP mutations (ArcSwe) (*18*). Further, ^{124}I-RmAb158-scFv8D3 also enabled monitoring of Aβ brain levels following Aβ reducing treatment with BACE-1 inhibitor NB-360 (*6, 19*) in a cross-sectional study design in ArcSwe mice of 10 months, i.e. an age associated with limited Aβ accumulation. However, in the clinical situation, it is likely that most AD cases remain undetected until clinical symptoms such as memory impairment appear. Consequently, a disease modifying treatment will realistically be applied at a disease stage associated with advanced brain Aβ accumulation. Thus, diagnostic and dynamic biomarkers reflecting pathological changes covering also middle to late disease stage are required.

The aim of this study was to compare the ability of the clinically established radioligand ^{11}C-PiB and the novel protofibril selective radioligand ^{124}I-RmAb158-scFv158 to detect and quantify effects of anti-Aβ intervention using BACE-1 inhibitor NB-360 as a model drug. The study was performed in two different models: 1) the ArcSwe mouse model that shows ^{11}C-PiB positivity between the age of 12 and 18 months (*9, 20*) and 2) in the *App*$^{NL-G-F}$ knock-in mouse

model harboring the Arctic, Swedish and Iberian (APP I716F) mutations that is characterized by diffuse Aβ pathology that is not readily detected by amyloid imaging with PET (*21*). By inclusion of old mice, characterized by abundant brain Aβ pathology, the study was designed to resemble the disease stage when patients are likely to be diagnosed and potentially enrolled into clinical trials of novel drug candidates.

MATERIALS AND METHODS

Animals and Treatment

All experiments were performed according to the rules and regulations of the Swedish Animal Welfare Agency that are in line with the European Communities Council Directive since September 22, 2010. The experiments were approved by the Uppsala University Animal Ethics board (5.8.18-13350/2017). ArcSwe mice (*22*), at the age of 16 months, were administered BACE-1 inhibitor NB-360 (*6*) (Novartis) nutrition pellets (0.5 g NB-360 /kg_pellet) during 2 months. $App^{NL\text{-}G\text{-}F}$ mice (*23*), with an earlier onset of Aβ deposition, were treated between the age of 8 and 10 months. NB-360 treated groups were compared to age-matched groups that received only vehicle food, and further, to baseline groups reflecting pathology levels at the beginning of the treatment. In total 44 ArcSwe (baseline: n=15; NB-360: n=15; control: n=14) and 17 $App^{NL\text{-}G\text{-}F}$ mice (baseline: n=5; NB-360: n=6; control: n=6) were included in the study. Two wild type (WT) mice, 8 months, i.e. age-matched to the $App^{NL\text{-}G\text{-}F}$ baseline mice, were also included as a comparison (Study design shown in Supplementary Fig. 1 and animal information in Supplementary Table 1). In addition to the mice that underwent *in vivo* imaging, a separate group of mice, ArcSwe (n=2; 18 month) and $App^{NL\text{-}G\text{-}F}$ (n=2; 10 months) were used for *ex vivo* autoradiography. Mice had free access to food and water during the study.

Radiochemistry

PiB synthesis

^{11}C-PiB was synthesized using a previously described method with slight modifications related to automation using an in-house built synthesis device (TPS) (*24*). The final product was reformulated using solid phase extraction in approximately 10% ethanol in phosphate-buffered saline (PBS). ^{11}C-PiB was produced with a radioactivity yield of 2.1 ± 1.0 GBq (range 0.7-4.3 GBq), molar activity 33 ± 38 MBq/nmol, and a radiochemical purity of >99% at the end of the synthesis.

Antibody Labelling

RmAb158-scFv8D3 was labeled using direct radioiodination (*25*) as previously described (*18*). Iodine-124 (^{124}I) (PerkinElmer inc.) labelling was done in eight batches; 80 µg of RmAb158-scFv8D3 was labelled with 101.9 ± 16.6 MBq resulting in an average yield of about 75.7 ± 2.5%. A similar procedure was used for iodine-125 (^{125}I) labeling of RmAb158-scFv8D3 (*26*); 80 µg of RmAb158-scFv8D3 was labelled with 38.2 ± 4.3 MBq ^{125}I resulting in an average yield of 71.7 ± 3.6%.

PET/SPECT Imaging

All mice underwent a ^{11}C-PiB PET scan. ArcSwe mice were injected with 13.2 ± 3.6MBq ^{11}C-PiB with a molar activity of 19.0 ± 9.3 MBq/nmol. *App*$^{NL-G-F}$ mice were injected with 20.1 ± 6.6 MBq/nmol ^{11}C-PiB with a molar activity of 6.7 ± 1.6 MBq/nmol. Animals were either injected at the start of the PET scan and scanned for 1 h or injected 30 min prior to the PET scan and kept under anesthesia until start of a 30 min scan. For all animals, analysis of ^{11}C-PiB brain retention was performed using data acquired 40-60 min post injection.

Within a week after their ^{11}C-PiB PET scan, ArcSwe animals were PET scanned with ^{124}I-RmAb158-scFv8D3 and *App*$^{NL-G-F}$ mice were SPECT scanned with ^{125}I-RmAb158-scFv8D3. One day before injection with radiolabelled RmAb158-scFv8D3, mice were given drinking water

containing 0.5% sodium iodine (NaI) to reduce thyroidal uptake of ^{124}I and ^{125}I. After injection, the concentration was decreased to 0.2% NaI until the PET or SPECT scan. ArcSwe and *App*$^{NL-G-F}$ mice were injected with 11.6 ± 2.7 MBq ^{124}I-RmAb158-scFv8D3 and 7.2 ± 1.1 MBq ^{125}I-RmAb158-scFv8D3, respectively, and scanned 4 days post injection. The molar activities were 185.4 ± 28.7 MBq/nmol and 144.5 ± 8.8 MBq/nmol for the iodine-124 and the iodine-125 labelled radioligand, respectively. After PET/SPECT scanning, mice underwent transcardial perfusion with 40 ml 0.9% NaCl during 2.5 min. The brain was then isolated and divided into right and left hemispheres and the cerebellum was removed from the left hemisphere. Radioactivity was measured in the three brain samples (right hemisphere, left hemisphere without cerebellum and cerebellum from the left hemisphere) with a Wizard 2470 gamma counter (GE healthcare). All samples were frozen on dry ice and stored at -80 °C until further processing.

PET scans were either performed in a Triumph Trimodality System (TriFoil Imaging, Inc.) or a nanoScan system PET/MRI (Mediso). All PET scans performed with the Mediso system were reconstructed with a Tera-Tomo™ 3D algorithm (Mediso) with 4 iterations and 6 subsets. Data obtained with the Triumph system was reconstructed using a 3-dimensional ordered-subsets expectations maximization with 20 iterations. SPECT scans were performed with a nanoScan system SPECT/CT (Mediso) with 4 detectors at a frame time of 80 s. Images were reconstructed with a Tera-Tomo™ 3D algorithm (Mediso) with 48 iterations and 3 subsets. Each mouse was CT examined after the PET/SPECT scan.

All subsequent processing of the images was performed with Amide version 1.0.4 (*27*). CT and PET scans were manually aligned with a T2-weighted mouse brain atlas (*28*) to quantify activity in regions of interest (Supplementary Fig. 2).

Immunostaining and Autoradiography

Right brain hemispheres of PET/SPECT scanned animals were cryo-sectioned (20 µm) for anti-Aβ1-42 chromogen staining described previously (*18*) using the primary polyclonal

rabbit-anti-Aβ1-42 antibody (Agrisera). Triple immunofluorescence staining of Aβ, Iba-1 and GFAP and autoradiography was performed as previously described (*18*). Images were processed as described in Gustavsson et al. 2020 (*26*).

Brain Sample Preparation

Sequential extraction of brain tissue was performed as previously described (*29*) according to Table 1, using a Precellys Evolution system (Bertin Corp.) (4x10 s at 5500 rpm).

Biochemical Quantifications of Brain Tissue

Brain extraction samples (Table 1) were quantified with Enzyme-linked Immunosorbent Assay (ELISA) as previously described (*20, 30*). Assay details are displayed in (Table 2).

^{11}C-PiB Nuclear Track Emulsion and Autoradiography

A separate group of mice were injected with 18-20 MBq ^{11}C-PiB followed by transcardial perfusion at 20 or 40 min after injection. The brain was immediately removed and divided into right and left hemisphere. Brain samples were frozen on dry ice and processed into 20 µm sagittal sections for nuclear track emulsion (NTE) and 40 µm for *ex vivo* autoradiography. Prior to NTE, sections were stained for 2 min with saturated Thioflavin-S in 80% ethanol, washed 1 min in 70% ethanol and rinsed with PBS. NTE was performed as previously described (*29*). Exposure of the slides was started 30 min post perfusion (i.e. equal to 1.5 decay half-lives of carbon-11). The signal was developed after 2 hours. Images were acquired with a LSM700 confocal laser scanning microscope (Zeiss) and processed with Zen Zeiss software. Images were compiled with Adobe Photoshop 2020. Brain sections from the same animals were also exposed to a phosphor imaging plate (Fujifilm) within 20 min post perfusion. Plates were exposed for 80 min and read with an Amersham Typhoon imager (GE healthcare).

Statistics

Data was analyzed and plotted with GraphPad Prism 6. Groups were compared with one-way ANOVA using Bonferroni's post hoc test. Results are reported as mean ± standard deviation. *: P < 0.05, **: P < 0.01, ***: P < 0.001, ****: P<0.0001.

RESULTS

ArcSwe and *App*$^{NL-G-F}$ mice, treated with BACE-1 inhibitor NB-360 or with vehicle, were PET scanned with ^{11}C-PiB followed by a ^{124}I-RmAb158-scFv8D3 PET scan or a ^{125}I-RmAb158-scFv8D3 SPECT scan. Based on visual interpretation of PET images, ^{11}C-PiB retention in ArcSwe animals seemed slightly increased in the NB-360 and vehicle groups compared to the 2 months younger baseline group (Fig. 1A). When quantified as standard uptake value (SUV), a similar trend was observed in hippocampus (Hpc), cortex (Ctx), thalamus (Thl) and cerebellum (Cer), but the difference was not significant and inter-animal variation was large (Fig. 1B). ^{11}C-PiB retention in *App*$^{NL-G-F}$ mice was alike in all three groups (Fig. 1C). When quantified as SUV, inter-individual variation was high and differences between the three groups and WT were not significant (Fig. 1D). In summary, neither of the mouse models showed a significant difference in ^{11}C-PiB signal between the different groups, despite a trend towards an increased signal in older mice, i.e. after the two-month treatment period (both vehicle and NB-360), compared to baseline mice. Whole body PET images are shown in the supplementary (Supplementary Fig. 3).

^{124}I-RmAb158-scFv8D3 retention in NB-360 treated animals was clearly lower compared to vehicle animals, while there was no notable difference compared to baseline animals (Fig. 1A). Radioligand concentrations was significantly lower in Thl (P=0.049) of NB-360 treated animals compared to vehicle animals (Fig. 1B). The same trend was observed in Ctx, Hpc and Cer but did not reach significance. Vehicle animals displayed increased levels compared to baseline (Hpc: P=0.028; Ctx: P=0.018; Thl: P=0.021; Cer: P=0.039). Akin to results in ArcSwe animals, SPECT images revealed lower ^{125}I-RmAb158-scFv8D3 retention in *App*$^{NL-G-F}$ animals

treated with NB-360 compared with the vehicle group (Fig. 1C). When quantified, radioligand concentration was significantly lower in Hpc (P=0.017), Ctx (P=0.047) and Cer (P<0.001) (Fig. 1D). Vehicle animals displayed increased ^{125}I-RmAb158-scFv8D3 concentrations in Hpc (P=0.008) and Thl (P=0.047) compared to baseline.

^{11}C-PiB binding was also assessed in postmortem brain tissue with *ex vivo* autoradiography and compared to Aβ42 immunostaining of the adjacent brain sections (Fig. 2A). At 40 min after injection, ArcSwe animals showed ^{11}C-PiB binding in regions with abundant Aβ pathology such as Hpc, Ctx and Thl. White matter binding was observed in in Cer, corpus callosum, pons and medulla (Fig. 2A). *App*$^{NL-G-F}$ mice displayed low ^{11}C-PiB binding in Hpc, Ctx and Thl despite Aβ pathology, but in line with observations in ArcSwe animals, distinct white matter binding. ^{11}C-PiB binding in the Ctx was further investigated with NTE (Fig. 2B). At 20 min after ^{11}C-PiB injection in ArcSwe mice, the radioligand was evenly distributed in the tissue including the core of ThS stained Aβ deposits while at 40 min after injection, the radioligand was primarily localized around the dense core of ThS stained Aβ plaques. ^{11}C-PiB retention in *App*$^{NL-G-F}$ mice at 40 min post injection was lower than that observed in ArcSwe brain, but when present, also localized around the cores of ThS positive Aβ deposits.

Ex vivo autoradiography with radiolabeled RmAb158-scFv8D3 visualized the presence of the ligand in most parts of the brain. There was especially high retention of the radioligand in Ctx, Hpc and Thl already in the baseline groups in both ArcSwe and *App*$^{NL-G-F}$ mice (Fig. 3A). The spatial distribution of the radioligand did not change due to NB-360 or vehicle treatment, but the intensity of the radioactive signal was lower in the NB-360 and baseline ArcSwe and *App*$^{NL-G-F}$ mice compared to vehicle treated animals. This trend was also evident when the complete *post mortem* right hemispheres (from which brain sections were prepared) were measured in a gamma counter, although the difference did not reach significance due to large inter-individual variation (Fig. 3B). Aβ42 staining visualized Aβ affected brain regions, and further,

the overlap between pathology rich brain regions and radiolabelled RmAb158-scFv8D3 strongly indicated a co-localization between the radioligand and Aβ affected regions in both mouse models (Fig. 3A). NTE in combination with triple staining of GFAP, Iba1 and Aβ is shown in the supplementary (Supplementary Fig. 4).

Brain homogenates of all animals that underwent PET or SPECT were biochemically assessed with ELISA. TBS-soluble Aβ aggregates were quantified after centrifugation at 16 000xg and 100 000xg (Fig. 4A and D). In the 16 000xg fractions, NB-360 treated ArcSwe animals showed lower levels of Aβ aggregates compared to the vehicle group (P=0.0029) while this difference was not significant in the *App*$^{NL-G-F}$ mice (P>0.99). However, this decrease was more distinctive and significant in both animal models in the 100 000xg fraction (P<0.0001) representing smaller and more soluble aggregates. In addition, the NB-360 groups displayed lower Aβ levels in 100 000xg fractions compared to the baseline groups (P<0.0001). Aβ1-40 and Aβ1-42 in the formic acid extraction represents TBS insoluble Aβ, including fibrils, and thus represents total plaque load (Fig.4B and E). NB-360 treated *App*$^{NL-G-F}$, but not ArcSwe, displayed lower Aβ1-40 levels than vehicle treated animals, while Aβ1-42 levels were decreased in NB-360 treated animals compared to vehicle animals in both models. Correlations between PET/SPECT SUV and Aβ levels are included in the supplementary (Supplementary Table 2-5). Microglial activation was assessed by quantification of soluble triggering receptor expressed on myeloid cells 2 (sTREM2) in the 16 000xg fraction (Fig. 4C and F). BACE-1 inhibition decreased sTREM2 levels compared to vehicle in both models (P<0.0001). In the ArcSwe animals, that showed higher sTREM2 levels than the *App*$^{NL-G-F}$ animals at baseline, NB-360 treatment also reduced sTREM2 levels compared to baseline (P=0.0143).

DISCUSSION

Amyloid imaging has become an important inclusion criterion in clinical trials of candidate drugs aimed at reducing brain Aβ. Established amyloid radioligands, such as ^{11}C-PiB

bind to Aβ fibrils deposited as insoluble plaques in the AD brain. These established radioligands may therefore be insufficient for monitoring changes in more soluble or diffuse forms of misfolded and aggregated Aβ, which are likely to be affected first by anti-Aβ drugs. In this study we demonstrated that radiolabeled bispecific antibody RmAb158-scFv8D3, binding to soluble Aβ aggregates, was able to quantify changes in brain Aβ levels after treatment with BACE-1 inhibitor NB-360 in two mouse models of Aβ pathology, and further, that the read-out was different from that of ^{11}C-PiB PET, which did not detect any differences between treated and untreated groups.

The NB-360 treatment was started at an age when Aβ brain pathology was already advanced and the brain tissue, at least in the ArcSwe mice, included large amounts of dense cored Aβ deposits. Thus, it may not be surprising that the ^{11}C-PiB signal did not decrease with treatment as these deposits are likely to be very difficult to dissolve. In line with this observation, formic acid soluble Aβ1-40, the main constituent of dense core deposits (*31*), displayed the smallest difference between treatment groups. However, it was somewhat surprising that despite BACE-1 inhibition, leading to a dramatic reduction of the smallest aggregates as shown by ELISA in the 100 000xg TBS fraction, the ^{11}C-PiB signal tended to increase from baseline to the end of treatment. It implies that once insoluble deposits have been formed, they may continue to increase in number and size, especially if the “pool” of monomers and nonfibrillar aggregates has not been completely depleted. As illustrated by the ELISA measurements, the reduction in intermediate sized Aβ aggregates, i.e. the 16 000xg fraction, was either smaller than that observed for the soluble aggregates in the 100 000xg fraction (ArcSwe) or absent (*App*$^{NL-G-F}$). A longer treatment time may be required to remove also the 16 000xg aggregates. This hypothesis is supported by clinical studies of BACE-1 inhibitors that have reported decreased brain amyloid levels detected with PET after 1.5-2 years of treatment (*32, 33*).

The spatial distribution of ^{124}I-RmAb158-scFv8D3 studied by *ex vivo* autoradiography in combination with Aβ42 immunohistochemistry indicated radioligand

accumulation in Aβ rich brain regions in both mouse models. On the contrary, *ex vivo* autoradiography with ^{11}C-PiB was only evident in regions with abundant Aβ pathology in the ArcSwe model, but not in the *App*$^{NL\text{-}G\text{-}F}$ model. The main reason for selecting these two models for the present study was their dissimilar "Aβ profiles", illustrated by their very different relative ratios of Aβ40 and Aβ42; Aβ40 is the major Aβ species in ArcSwe mice while Aβ42 dominates in *App*$^{NL\text{-}G\text{-}F}$ mice (Fig. 4). It has been shown that although Aβ42 is more prone to aggregate, the dense core of plaques is formed by Aβ40 (*31*). It should also be noted that Aβ40 is the major Aβ isoform produced in human sporadic AD (*34*). Thus, this leads to another important aspect highlighted in the present study, i.e. the selection of animal models for preclinical studies of brain Aβ, especially when evaluating the ability of candidate drugs to reduce pathology. The application of ^{11}C-PiB, and analogues, in animal studies has indeed been debated over the last 10-15 years. First, preclinical attempts to quantify Aβ deposits with ^{11}C-PiB in the PS1/APP transgenic mouse model resulted in contradictory results claiming structural differences between Aβ plaque formation and cerebral pathology in mice and humans (*35*). Yet, more recent studies have demonstrated that Aβ deposits can be assessed by ^{11}C-PiB in mouse models such as APP23 (*36, 37*) and APP/PS1-21 (*38*). Further, several studies with ^{18}F labelled analogs of ^{11}C-PiB have underlined the ability of Aβ plaque assessment in different mouse models (*39*), especially in longitudinal studies (*21, 40*). Several studies have reported the ability of amyloid-PET to quantify disease modifying treatments, e.g. mApoE-pA-Lip in APP23 mice (*41*) and BACE-1 inhibition in PS2APP mice (*42*). Thus, the use of amyloid-PET likely requires a model with dense core Aβ deposits. The present study also demonstrated that weak ^{11}C-PiB binding is not *per see* a sign of low brain Aβ levels as radiolabeled RmAb158-scFv8D3 was readily able to detect the abundant Aβ pathology in "^{11}C-PiB negative" *App*$^{NL\text{-}G\text{-}F}$ mice both *in vivo* and *ex vivo*. In line with this, patients suffering from AD caused by specific mutations in the AβPP, with confirmed diffuse pathology and absence of dense core plaques, have also been reported as ^{11}C-PiB negative (*7*). Again, this illustrates the need for radioligands able to quantify Aβ in other forms than insoluble deposits (plaques).

We used SUV, i.e. activity concentrations normalized to the injected activity per bodyweight, as the main read-out measure from PET. This is different from the majority of studies that have reported SUVRs, i.e. activity ratios between regions of interest and a reference region. The reference region used in previous studies has in most cases been cerebellum or periaqueductal grey (*21*). However, in the present study, Aβ pathology was spread in the whole brain at the start of the study, and hence, excluding the use of a pathology-free region as reference. In addition, all brain regions, including cerebellum and PAG, were affected by disease progression and by NB-360 treatment as shown with PET/SPECT and autoradiography, and by ELISA of post mortem cerebellum homogenates (Supplementary Fig. 5). Thus, in this setting it was not possible to use reference region-based methods.

Apart from Aβ, brain sTREM2 concentrations were also investigated in brain homogenates and found to be decreased in both mouse models after administration of NB-360. This suggests an extenuating effect on microglia activation due to lower Aβ production and aggregation.

CONCLUSION

Antibody-based PET and SPECT imaging of soluble Aβ aggregates is a sensitive tool to follow Aβ pathology in the brain. This study demonstrates the ability of such ligands to quantify changes due to anti-Aβ treatment at a stage of advanced Aβ pathology. Thus, radioligands based on antibodies directed towards a specific form of aggregated Aβ may have potential to improve and complement diagnostics in preclinical and clinical studies of AD drug candidates. We demonstrate in this study that radiolabeled RmAb158-scFv8D3 is able to quantify changes in brain Aβ levels after BACE-1 inhibition in two AD mouse models, and further, that the read-out is different from that of ^{11}C-PiB.

DISCLOSURE

Ulf Neumann is an employee and shareholder of Novartis Pharma AG, Basel, Switzerland.

ACKNOWLEDGEMENTS

We thank Dr. Derya Shimshek, Novartis, for supplying the NB-360 food pellets; Professor Lars Nilsson for developing the ArcSwe mouse model used in this study and BioArctic for sharing the mAb158 sequence. This work was supported by grants from the Swedish Research Council (2017-02413, 2018-02715), Alzheimerfonden, Hjärnfonden, Torsten Söderbergs stiftelse, Åhlénstiftelsen, Magnus Bergwalls stiftelse, Stiftelsen för gamla tjänarinnor and Konung Gustaf V:s och Drottning Victorias Frimurarestiftelsen. The funding bodies did not take part in design of the study, in collection, analysis, or interpretation of data, nor in writing the manuscript. The molecular imaging work in this study was performed at the SciLifeLab Pilot Facility for Preclinical PET-MRI, a Swedish nationally available imaging platform at Uppsala University, Sweden, financed by the Knut and Alice Wallenberg Foundation.

KEY POINTS

QUESTION: Do ^{11}C-PIB and ^{124}I-antibody PET read-outs provide differing estimates of brain Aβ after therapeutic intervention in ArcSwe and *App*$^{NL-G-F}$ mice with pronounced Aβ pathology? And if they do, what is the implication for drug development for AD?

PERITENT FINDINGS: The antibody-based radioligand detected changes in brain Aβ levels after anti-Aβ therapy in ArcSwe and *App*$^{NL-G-F}$ mice. In contrast, the decreased Aβ levels could not be quantified with “gold standard” ^{11}C-PiB PET, suggesting that these ligands detect different pools of the Aβ.

IMPLICATION FOR PATIENT CARE: Radioligands based on antibodies directed towards a specific form of aggregated Aβ may have potential to improve and complement diagnostics in preclinical and clinical studies of AD drug candidates.

REFERENCES

1. Ziegler-Graham K, Brookmeyer R, Johnson E, Arrighi HM. Worldwide variation in the doubling time of Alzheimer's disease incidence rates. *Alzheimers Dement*. 2008;4:316-323.

2. Chételat G, La Joie R, Villain N, et al. Amyloid imaging in cognitively normal individuals, at-risk populations and preclinical Alzheimer's disease. *Neuroimage: Clin*. 2013;2:356-365.

3. Engler H, Forsberg A, Almkvist O, et al. Two-year follow-up of amyloid deposition in patients with Alzheimer's disease. *Brain*. 2006;129:2856-2866.

4. Esparza TJ, Wildburger NC, Jiang H, et al. Soluble Amyloid-beta Aggregates from Human Alzheimer's Disease Brains. *Sci Rep*. 2016;6:38187.

5. Keskin AD, Kekuš M, Adelsberger H, et al. BACE inhibition-dependent repair of Alzheimer's pathophysiology. *Proc Natl Acad Sci USA*. 2017;114:8631-8636.

6. Neumann U, Rueeger H, Machauer R, et al. A novel BACE inhibitor NB-360 shows a superior pharmacological profile and robust reduction of amyloid-β and neuroinflammation in APP transgenic mice. *Mol Neurodegener*. 2015;10:44.

7. Schöll M, Wall A, Thordardottir S, et al. Low PiB PET retention in presence of pathologic CSF biomarkers in Arctic APP mutation carriers. *Neurology*. 2012;79:229-236.

8. Englund H, Sehlin D, Johansson A-S, et al. Sensitive ELISA detection of amyloid-β protofibrils in biological samples. *J Neurochem*. 2007;103:334-345.

9. Fang XT, Hultqvist G, Meier SR, Antoni G, Sehlin D, Syvänen S. High detection sensitivity with antibody-based PET radioligand for amyloid beta in brain. *Neuroimage*. 2019;184:881-888.

10. Sehlin D, Fang XT, Meier SR, Jansson M, Syvänen S. Pharmacokinetics, biodistribution and brain retention of a bispecific antibody-based PET radioligand for imaging of amyloid-β. *Sci Rep*. 2017;7:17254.

11. Sehlin D, Stocki P, Gustavsson T, et al. Brain delivery of biologics using a cross-species reactive transferrin receptor 1 VNAR shuttle. *FASEB J*. 2020.

12. Syvänen S, Fang XT, Hultqvist G, Meier SR, Lannfelt L, Sehlin D. A bispecific Tribody PET radioligand for visualization of amyloid-beta protofibrils - a new concept for neuroimaging. *Neuroimage*. 2017;148:55-63.

13. Sehlin D, Syvänen S. Engineered antibodies: new possibilities for brain PET? *Eur J Nucl Med Mol Imaging*. 2019;46:2848-2858.

14. Hultqvist G, Syvänen S, Fang XT, Lannfelt L, Sehlin D. Bivalent Brain Shuttle Increases Antibody Uptake by Monovalent Binding to the Transferrin Receptor. *Theranostics*. 2017;7:308-318.

15. Lord A, Gumucio A, Englund H, et al. An amyloid-beta protofibril-selective antibody prevents amyloid formation in a mouse model of Alzheimer's disease. *Neurobiol Dis*. 2009;36:425-434.

16. Logovinsky V, Satlin A, Lai R, et al. Safety and tolerability of BAN2401--a clinical study in Alzheimer's disease with a protofibril selective Aβ antibody. *Alzheimers Res Ther*. 2016;8:14.

17. Lee HJ, Engelhardt B, Lesley J, Bickel U, Pardridge WM. Targeting Rat Anti-Mouse Transferrin Receptor Monoclonal Antibodies through Blood-Brain Barrier in Mouse. *J Pharmacol Exp Ther*. 2000;292:1048-1052.

18. Meier SR, Syvänen S, Hultqvist G, et al. Antibody-Based In Vivo PET Imaging Detects Amyloid-β Reduction in Alzheimer Transgenic Mice After BACE-1 Inhibition. *J Nucl Med*. 2018;59:1885-1891.

19. Neumann U, Machauer R, Shimshek DR. The β-secretase (BACE) inhibitor NB-360 in preclinical models: From amyloid-β reduction to downstream disease-relevant effects. 2019;176:3435-3446.

20. Sehlin D, Fang XT, Cato L, Antoni G, Lannfelt L, Syvänen S. Antibody-based PET imaging of amyloid beta in mouse models of Alzheimer's disease. *Nat Commun*. 2016;7:10759.

21. Sacher C, Blume T, Beyer L, et al. Longitudinal PET monitoring of amyloidosis and microglial activation in a second-generation amyloid-β mouse model. *J Nucl Med*. 2019;60:1787-1793.

22. Lord A, Kalimo H, Eckman C, Zhang X-Q, Lannfelt L, Nilsson LNG. The Arctic Alzheimer mutation facilitates early intraneuronal Abeta aggregation and senile plaque formation in transgenic mice. *Neurobiol Aging*. 2006;27:67-77.

23. Saito T, Matsuba Y, Mihira N, et al. Single App knock-in mouse models of Alzheimer's disease. *Nat Neurosci*. 2014;17:661-663.

24. Klunk WE, Engler H, Nordberg A, et al. Imaging brain amyloid in Alzheimer's disease with Pittsburgh Compound-B. *Ann Neurol*. 2004;55:306-319.

25. Greenwood FC, Hunter WM, Glover JS. The preparation of 131I-labelled human growth hormone of high specific radioactivity. *Biochem J*. 1963;89:114-123.

26. Gustavsson T, Syvänen S, O'Callaghan P, Sehlin D. SPECT imaging of distribution and retention of a brain-penetrating bispecific amyloid-β antibody in a mouse model of Alzheimer's disease. *Transl Neurodegener*. 2020;9:37.

27. Andreas Markus Loening SSG. AMIDE: a free software tool for multimodality medical image analysis. *Mol Imaging*. 2003;2:131-7.

28. Ma Y, Hof PR, Grant SC, et al. A three-dimensional digital atlas database of the adult C57BL/6J mouse brain by magnetic resonance microscopy. *Neuroscience*. 2005;135:1203-1215.

29. Meier SR, Sehlin D, Hultqvist G, Syvänen S. Pinpointing Brain TREM2 Levels in Two Mouse Models of Alzheimer's Disease. *Mol Imaging Biol*. 2021:in press.

30. Sehlin D, Englund H, Simu B, et al. Large aggregates are the major soluble Aβ species in AD brain fractionated with density gradient ultracentrifugation. *PLOS ONE*. 2012;7:e32014.

31. Michno W, Wehrli P, Meier SR, et al. Chemical imaging of evolving amyloid plaque pathology and associated Aβ peptide aggregation in a transgenic mouse model of Alzheimer's disease. *J Neurochem*. 2020;152:602-616.

32. Egan MF, Kost J, Tariot PN, et al. Randomized Trial of Verubecestat for Mild-to-Moderate Alzheimer's Disease. *N Engl J Med*. 2018;378:1691-1703.

33. Phase II Clinical Study of Elenbecestat Demonstrates Safety and Tolerability in MCI and Mild to Moderate Alzheimer's Disease at 18-Months | Biogen.

34. Gregory GC, Halliday GM. What is the dominant Abeta species in human brain tissue? A review. *Neurotox Res*. 2005;7:29-41.

35. Klunk WE, Lopresti BJ, Ikonomovic MD, et al. Binding of the Positron Emission Tomography Tracer Pittsburgh Compound-B Reflects the Amount of Amyloid-β in Alzheimer's Disease Brain But Not in Transgenic Mouse Brain. *J Neurosci*. 2005;25:10598-10606.

36. Maeda J, Ji B, Irie T, et al. Longitudinal, Quantitative Assessment of Amyloid, Neuroinflammation, and Anti-Amyloid Treatment in a Living Mouse Model of Alzheimer's Disease Enabled by Positron Emission Tomography. *J Neurosci*. 2007;27:10957-10968.

37. Snellman A, López-Picón FR, Rokka J, et al. Longitudinal Amyloid Imaging in Mouse Brain with 11C-PIB: Comparison of APP23, Tg2576, and APPswe-PS1dE9 Mouse Models of Alzheimer Disease. *J Nucl Med*. 2013;54:1434-1441.

38. Maier FC, Wehrl HF, Schmid AM, et al. Longitudinal PET-MRI reveals β-amyloid deposition and rCBF dynamics and connects vascular amyloidosis to quantitative loss of perfusion. *Nat Med*. 2014;20:1485-1492.

39. Brendel M, Jaworska A, Grießinger E, et al. Cross-sectional comparison of small animal [18F]-florbetaben amyloid-PET between transgenic AD mouse models. *PLOS ONE*. 2015;10:e0116678.

40. Rominger A, Brendel M, Burgold S, et al. Longitudinal assessment of cerebral β-amyloid deposition in mice overexpressing Swedish mutant β-amyloid precursor protein using 18F-florbetaben PET. *J Nucl Med*. 2013;54:1127-1134.

41. Snellman A, Rokka J, López-Picón FR, et al. Applicability of [11C]PIB micro-PET imaging for in vivo follow-up of anti-amyloid treatment effects in APP23 mouse model. *Neurobiol Aging*. 2017;57:84-94.

42. Brendel M, Jaworska A, Overhoff F, et al. Efficacy of chronic BACE1 inhibition in PS2APP mice depends on the regional Aβ deposition rate and plaque burden at treatment initiation. *Theranostics*. 2018;8:4957-4968.

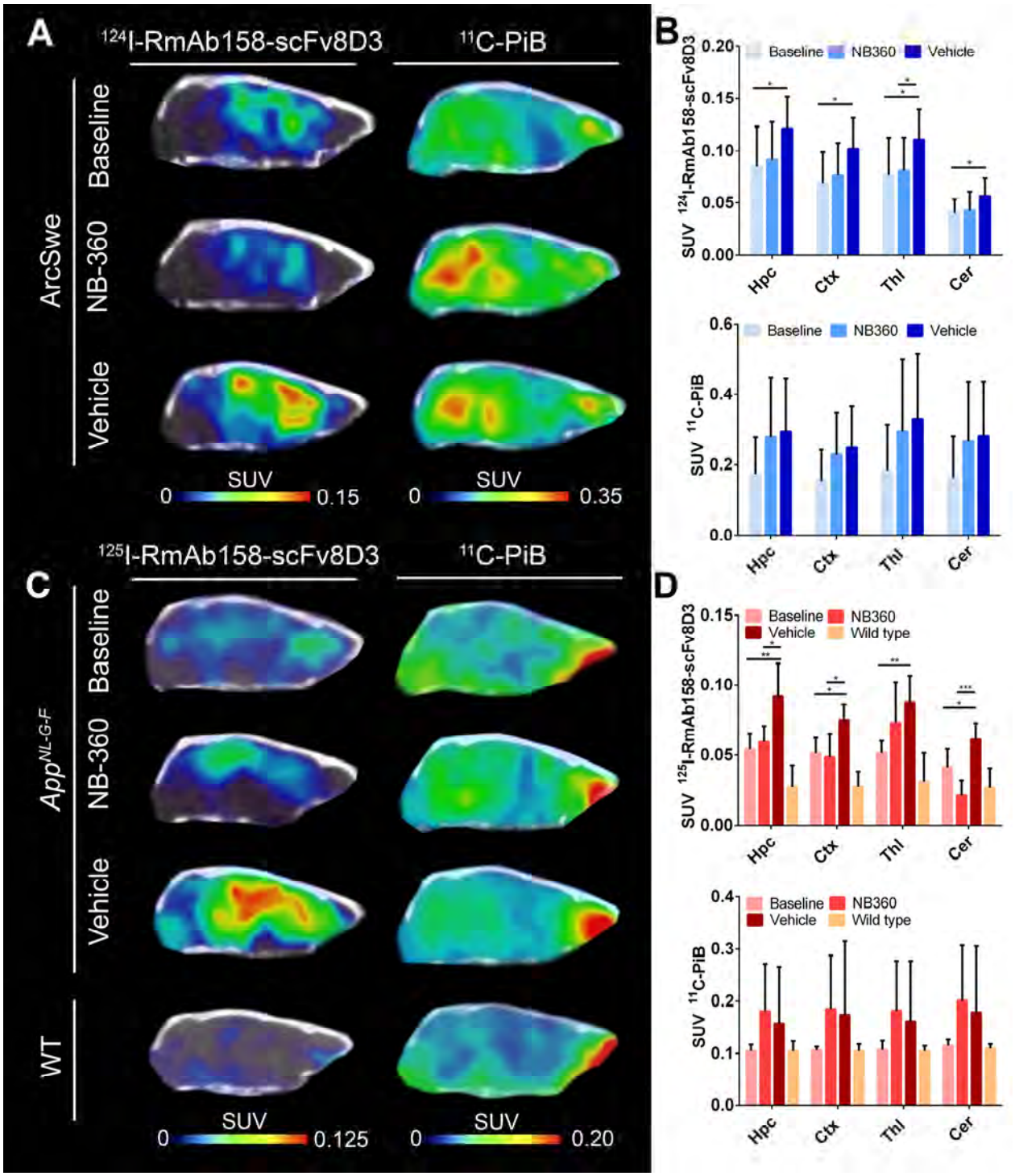

FIGURE 1. PET images and quantification of ^{11}C-PiB (40-60min after injection) and ^{124}I-RmAb158-scFv8D3 scans (72h after injection) expressed as standardized uptake value (SUV). (A): Comparison of representative ^{124}I-RmAb158-scFv8D3 and ^{11}C-PiB PET images in ArcSwe

animals. (B): Quantification of ^{124}I-RmAb158-scFv8D3 and ^{11}C-PiB in hippocampus (Hpc), cortex (Ctx), thalamus (Thl) and cerebellum (Cer). (C): Comparison of representative SPECT and PET images of ^{125}I-RmAb158-scFv8D3 and ^{11}C-PiB of *App*$^{NL-G-F}$ and WT animals. (D): Retention of ^{125}I-RmAb158-scFv8D3 and ^{11}C-PiB in different brain regions of *App*$^{NL-G-F}$ and WT animals.

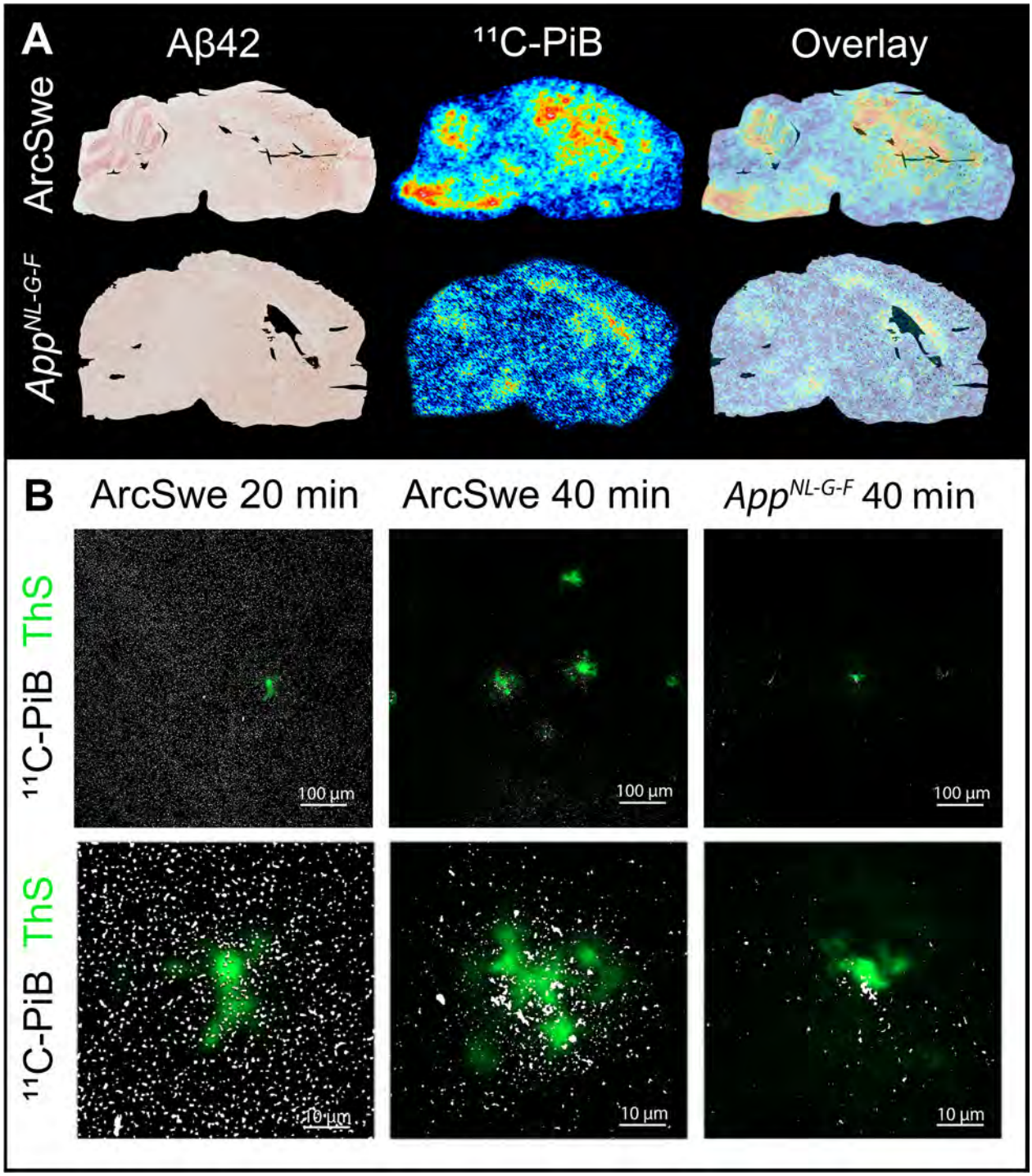

FIGURE 2. *Ex vivo* ^{11}C-PiB retention in postmortem brain tissue. (A): Aβ42 stained brain sections of an 18-month-old ArcSwe and a 10-month-old *App*$^{NL-G-F}$ mouse and corresponding *ex vivo* ^{11}C-PiB autoradiography images at 40 min after radioligand injection. The overlay illustrates the

overlap of regions with abundant Aβ plaque pathology and radioligand binding. (B): ThS staining (green) and nuclear track emulsion (NTE, white dots) of ^{11}C-PiB in ArcSwe and *App*$^{NL-G-F}$ mice.

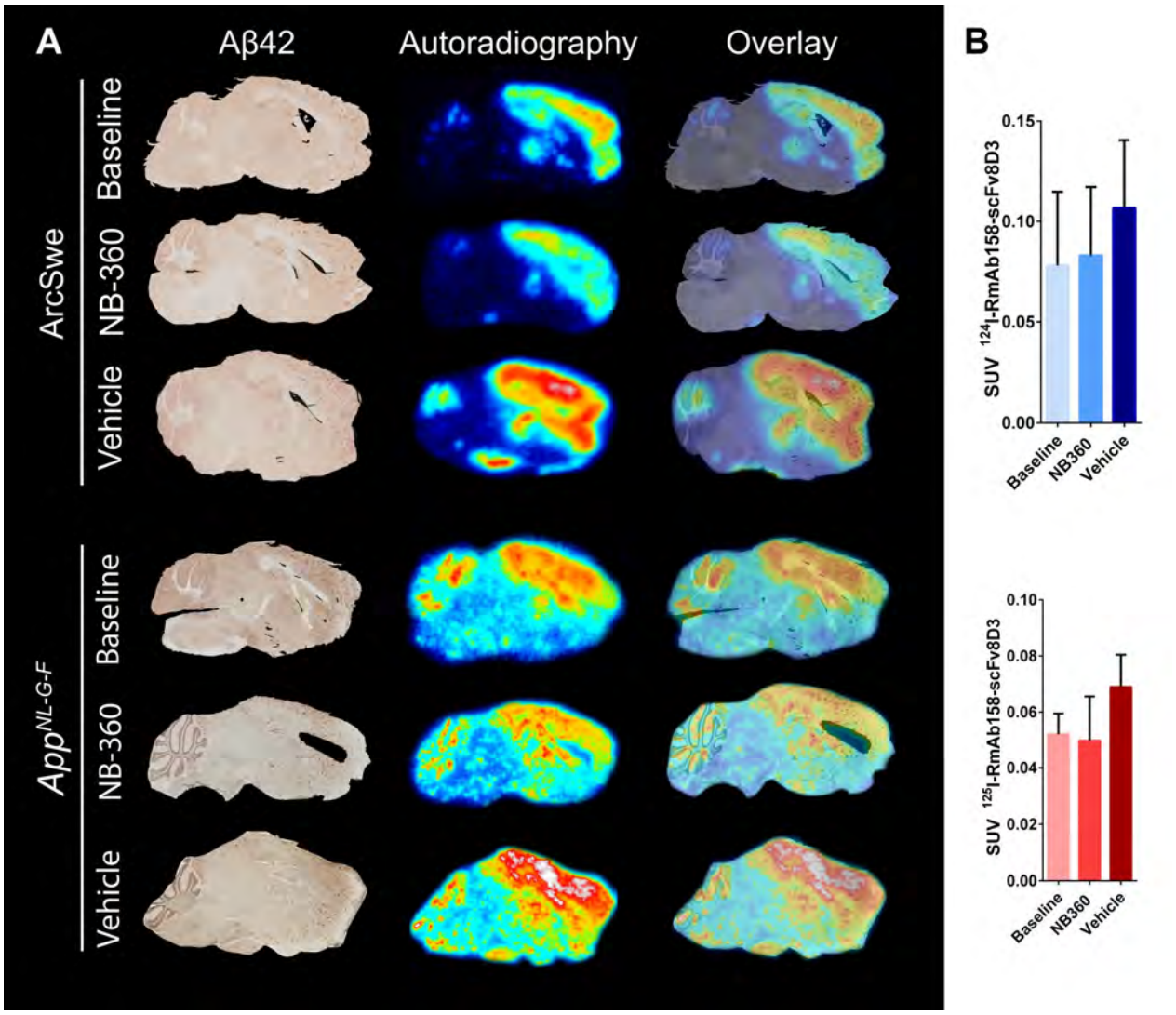

FIGURE 3. Aβ42 immunohistochemistry and *ex vivo* autoradiography of $^{124/125}$I-RmAb158-scFv8D3 in brain tissue. (A): Comparison of Aβ42 staining and autoradiography on sagittal brain sections of one representative ArcSwe or *App*$^{NL-G-F}$ animal of each studied group. The stained brain section was merged to an overlay with the corresponding *ex vivo* autoradiography of the same animal to visualize simultaneously the pathology and tracer binding. (B): Postmortem *ex vivo* quantification of $^{124/125}$I-RmAb158-scFv8D3 in the complete right hemisphere in ArcSwe and *App*$^{NL-G-F}$ animals.

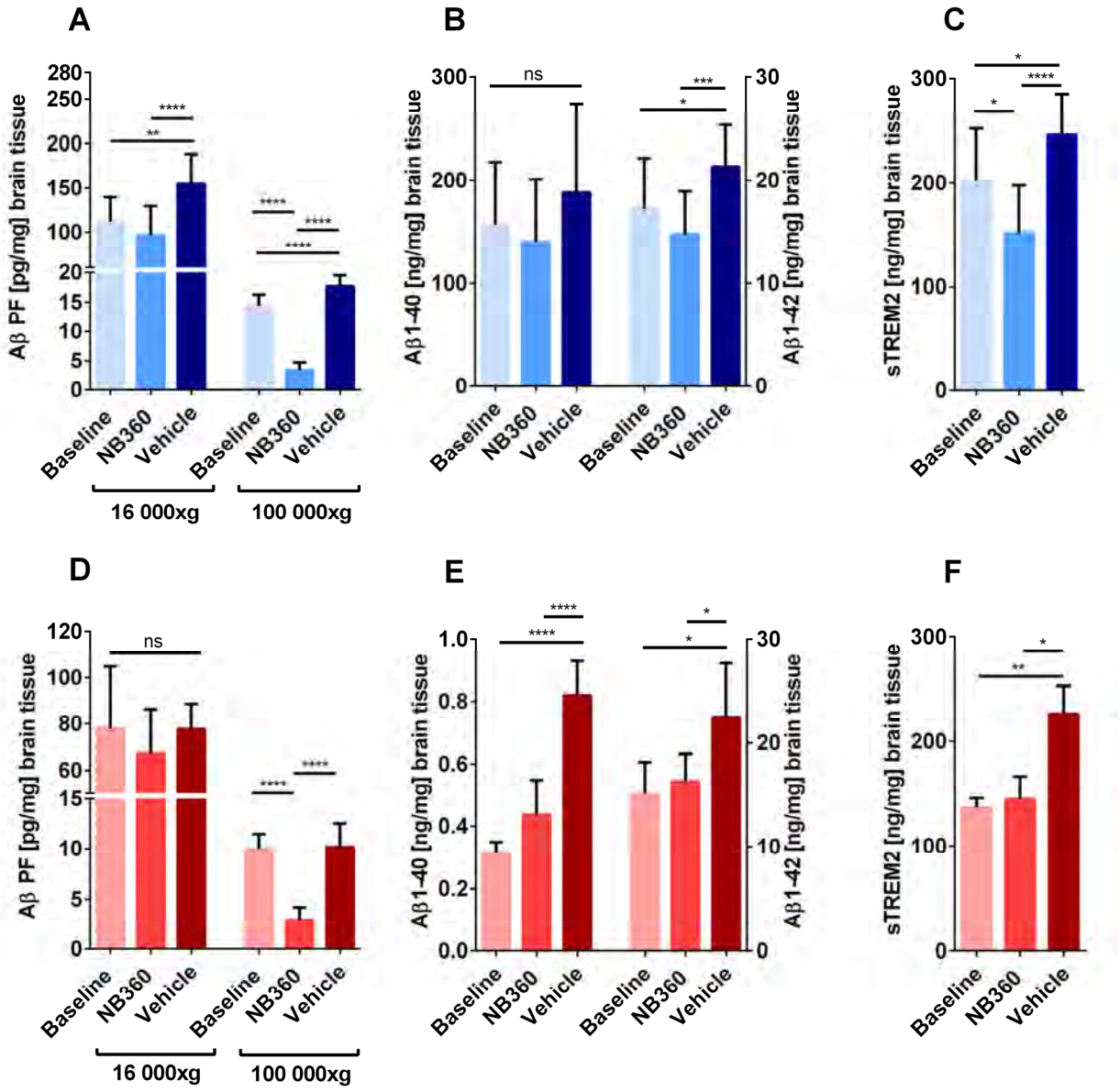

FIGURE 4. Quantification of Aβ and sTREM2 in brain homogenates. (A): Quantification of nonfibrillar, TBS soluble Aβ aggregates separated at 16 000xg and 100 000xg of ArcSwe brains separated at 16 000xg. (B): Insoluble Aβ1-40 and Aβ1-42 in formic acid extraction of ArcSwe brains. (C): sTREM2 levels in TBS extracted brain homogenates of ArcSwe animals (D): Quantification of nonfibrillar, TBS soluble Aβ aggregates separated at 16 000xg and 100 000xg of *App*$^{NL-G-F}$ animals. (E): Insoluble Aβ1-40 and Aβ1-42 in formic acid extraction of *App*$^{NL-G-F}$ brains.

extraction of *App*$^{NL\text{-}G\text{-}F}$ brains. (F): sTREM2 levels in TBS extracted brain homogenates of *App*$^{NL\text{-}G\text{-}F}$ animals.

Graphical Abstract

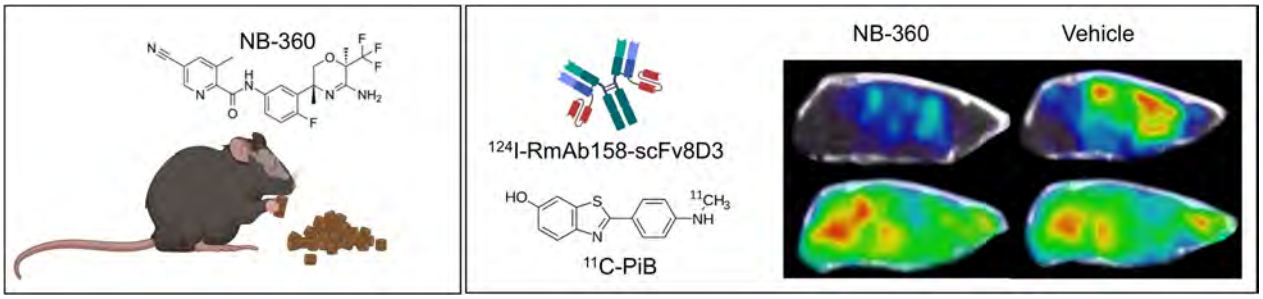

Tables

TABLE 1. Extractions performed on the brain tissue for ELISA analysis.

Step	Material	Extraction	Medium	Centrifugation
1	Fresh frozen brain tissue	1:5 weight:volume ratio of tissue	TBS	1 h, 16 000xg
2	Pellet TBS extraction (Step 1)	1:5 weight:volume ratio of tissue	70% formic acid (FA)	1 h, 16 000xg
3	TBS extract (Step 1)	200 µL TBS extract (Step 1)	TBS	1 h, 100 000xg

TABLE 2. Antibodies and extraction fractions used in ELISA analysis.

Target	Extraction Sample	Primary antibody	Secondary antibody	Distributor
Non-fibrillar Aβ aggregates	TBS, 16 000xg	mAb3D6	mAb3D6-bio	In-house expression
Small sized, non-fibrillar Aβ aggregates	TBS, 100 000xg	mAb3D6	mAb3D6-bio	In-house expression
Fibrillar Aβ1-40	FA, 16 000xg	Anti-Aβ40	mAb3D6-bio	Agrisera/ In-house expression
Fibrillar Aβ1-42	FA, 16 000xg	Anti-Aβ42	mAb3D6-bio	Invitrogen/ In-house expression
sTREM2	TBS, 16 000xg	AF1729	BAF1729	R&D Systems

Supplementary material

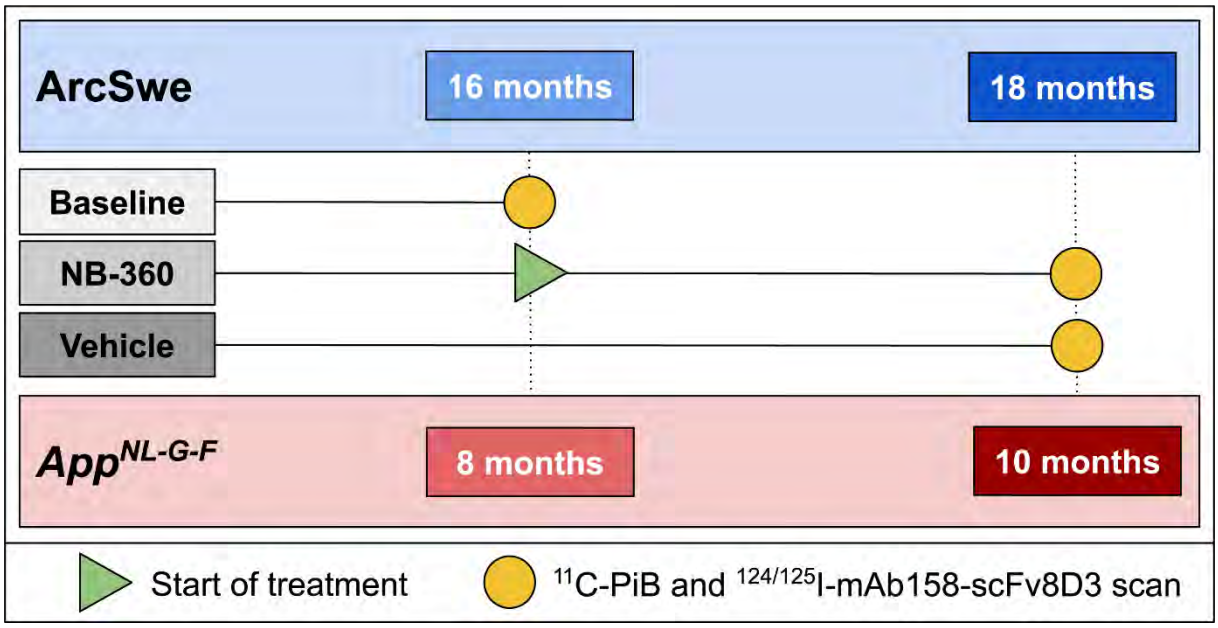

Supplementary FIGURE 1. Study design. The study compared three different groups within each mouse model. The NB-360 group received food containing BACE-1 inhibitor NB-360 for 2 months while vehicle animals were kept on control food. A third group was investigated at the age when BACE-1 inhibitor treatment was started to enable comparison to baseline. ArcSwe animals received BACE-1 treatment between 16 and 18 months while *App*$^{NL-G-F}$ mice were treated between 8 and 10 months. All mice were scanned with ^{11}C-PiB followed by an antibody scan with ^{124}I-RmAb158-scFv8D3 (ArcSwe) and ^{125}I-RmAb158-scFv8D3 (*App*$^{NL-G-F}$) at the end of the treatment period.

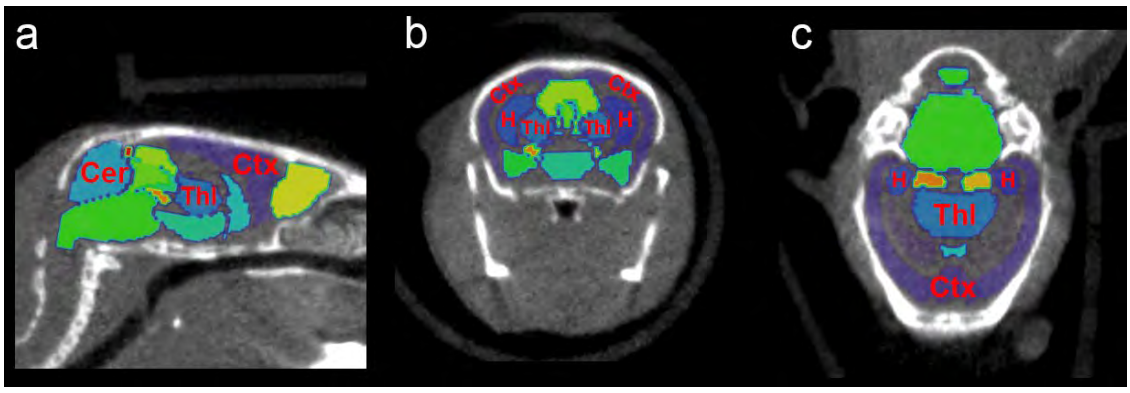

Supplementary Figure 2. Brain atlas

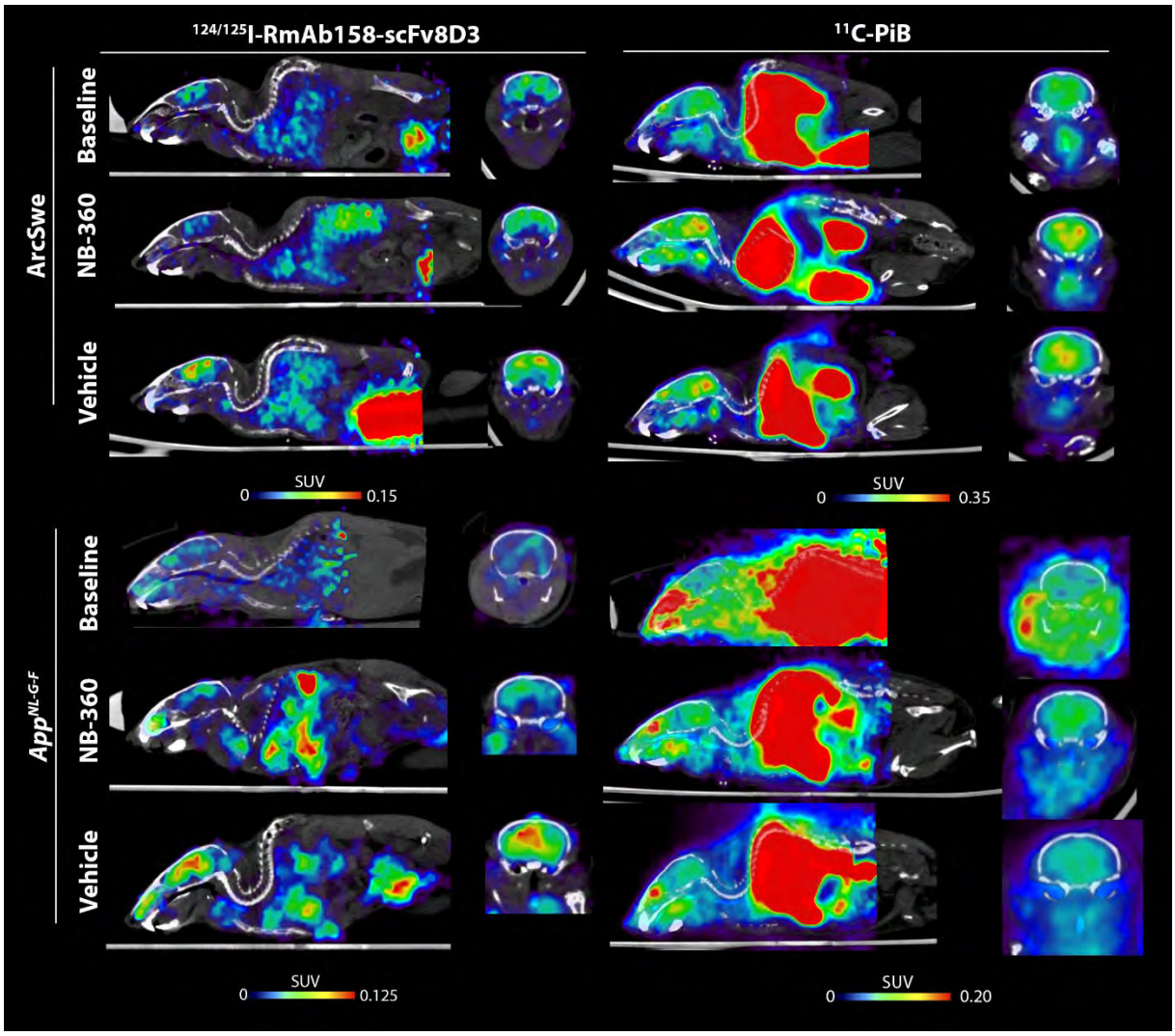

Supplementary Figure 3. Additional PET and SPECT images. Whole body and coronal view of representative animals of each group.

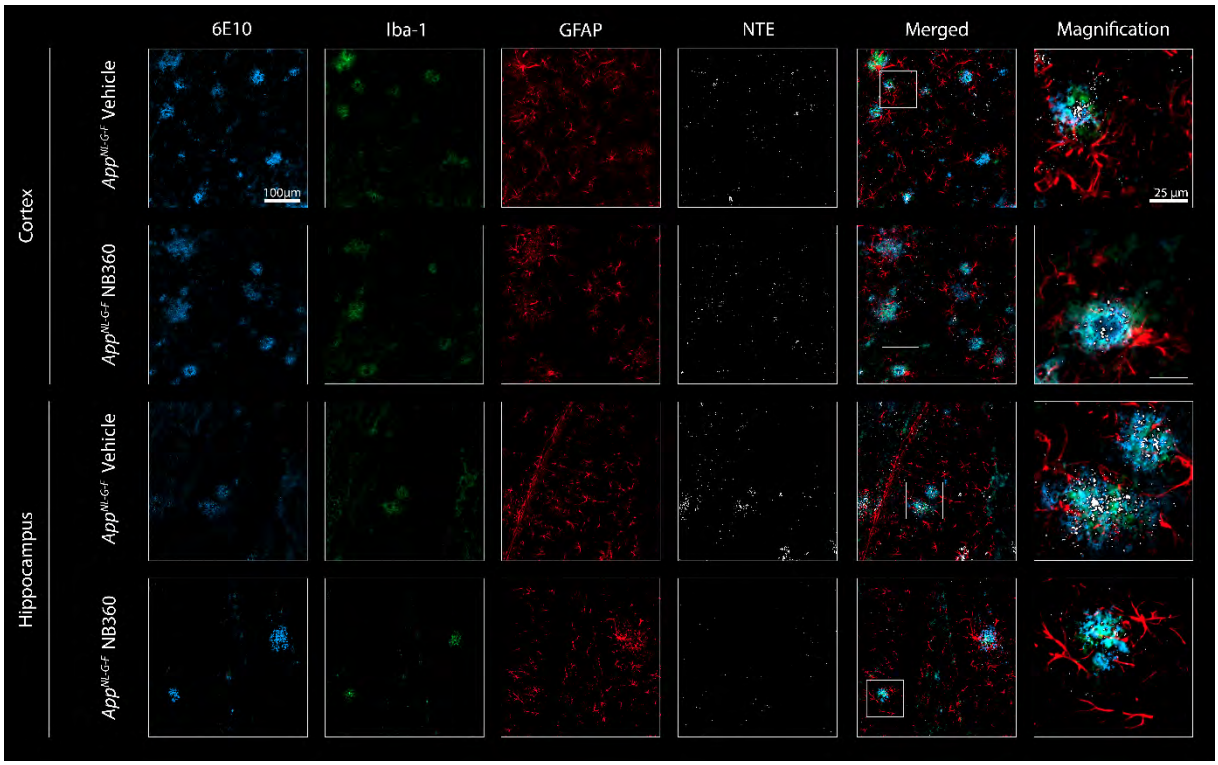

Supplementary Figure 4. Brain pathology. Triple staining of Aβ, Iba-1 (microglia), and GFAP (astrocytes) in combination with nuclear track emulsion (NTE) on brain sections prepared from *App*$^{NL-G-F}$ mice administered with ^{125}I-RmAb158-scFv8D3**.**

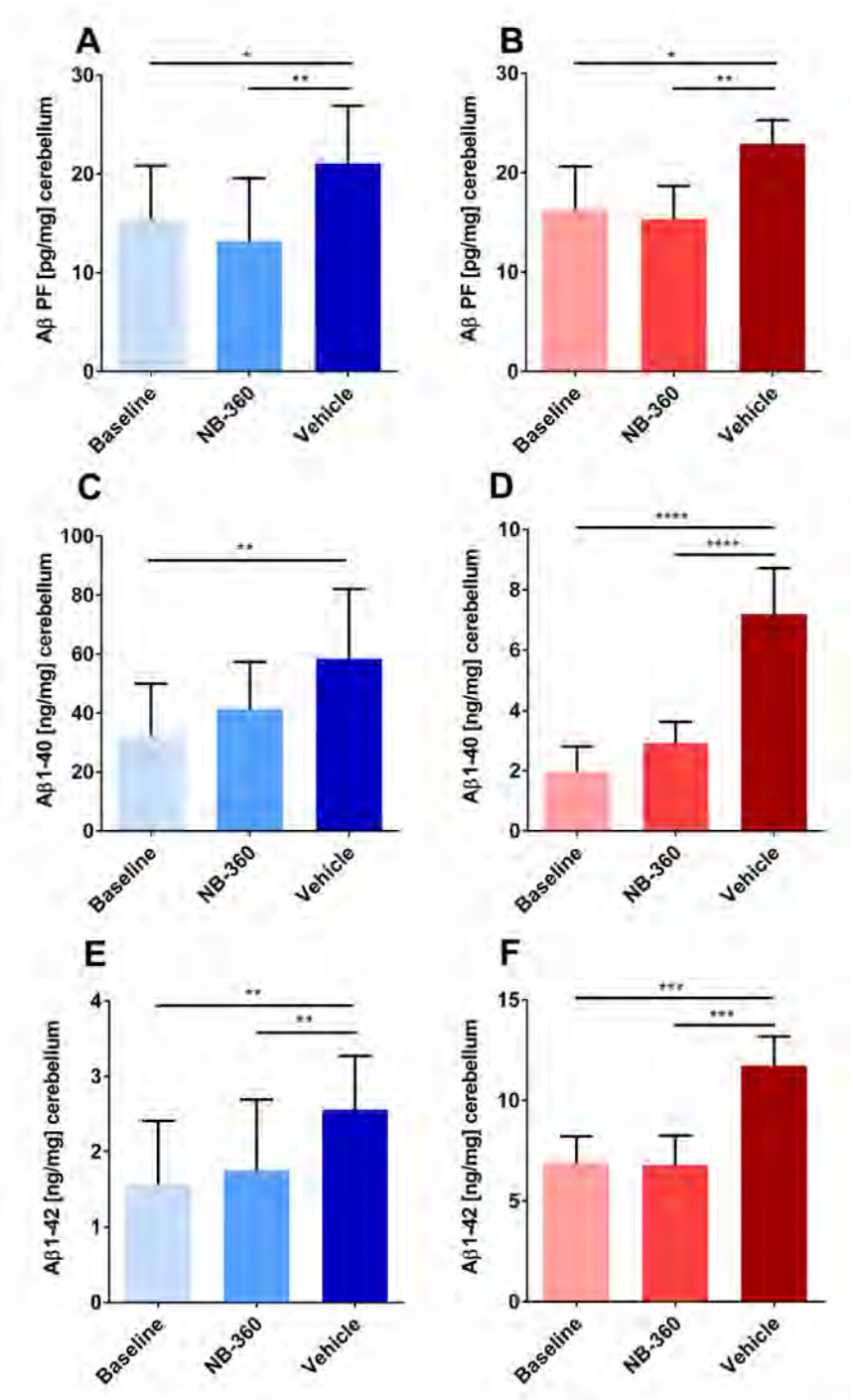

Supplementary Figure 5. **Biochemical quantification of cerebellum homogenates**. **(A)**: Quantification of TBS soluble Aβ aggregates in ArcSwe animals. **(B)**: Quantification of TBS soluble Aβ aggregates in *App*$^{NL\text{-}G\text{-}F}$ animals. **(C)**: Quantification of fibrillar Aβ1-40 extraction of ArcSwe animals. **D**: Quantification of fibrillar Aβ1-40 extraction in *App*$^{NL\text{-}G\text{-}F}$ animals. **(E)**: Quantification of fibrillar Aβ1-42 extraction of ArcSwe animals **(F)**: Quantification of fibrillar Aβ1-42 extraction in *App*$^{NL\text{-}G\text{-}F}$ animals.

Supplementary Table 1. Animals included in the study

Experimental group	Animal model	Age at euthanisation (months)	Number of animals (n)	Sex
Baseline	ArcSwe	16	15	8 ♀; 7 ♂
NB-360	ArcSwe	18	15	5 ♀; 10 ♂
Vehicle	ArcSwe	18	14	5 ♀; 9 ♂
Baseline	*App*$^{NL-G-F}$	8	5	3♀; 2♂
NB-360	*App*$^{NL-G-F}$	10	6	2♀; 4♂
Vehicle	*App*$^{NL-G-F}$	10	6	2♀; 4♂
Baseline	WT	8	2	1♀; 1♂
Autoradiography	ArcSwe	18	2	2♂
Autoradiography	*App*$^{NL-G-F}$	10	2	2♂

Supplementary Table 2. Correlation analysis of imaging and ELISA readouts in ArcSwe animals. Whole brain was used as the imaging readout. Values display the Pearson correlation coefficient (R). *: P < 0.05, **: P < 0.01, ***: P < 0.001, ****: P<0.0001.

	^{124}I-mAb158-scFv8D3	^{11}C-PiB	Aβ PF TBS 16 000xg	Aβ PF TBS 100 000xg	Aβ40 FA
Aβ42 FA	0.55 ****	0.21	0.65 ****	0.53 ***	0.53 ***
Aβ40 FA	0.57 ****	0.27	0.58 ****	0.27	
Aβ PF TBS 100 000xg	0.27	-0.03	0.60 ****		
Aβ PF TBS 16 000xg	0.61 ****	0.26			
^{11}C-PiB	0.32 *				

Supplementary Table 3. Correlation analysis of imaging and ELISA readouts in *App*$^{NL-G-F}$ animals. Whole brain was used as the imaging readout. Values display the pearson correlation coefficient (R). *:P < 0.05, **: P < 0.01, ***: P < 0.001, ****: P<0.0001.

	^{124}I-mAb158-scFv8D3	^{11}C-PiB	Aβ PF TBS 16 000xg	Aβ PF TBS 100 000xg	Aβ40 FA
Aβ42 FA	0.50 *	0.33	-0.07	0.32	0.82
Aβ40 FA	0.47	0.11	0.02	0.26	
Aβ PF TBS 100 000xg	0.42	-0.14	0.46		
Aβ PF TBS 16 000xg	-0.33	0.21			
^{11}C-PiB	-0.20				

Supplementary Table 4. Correlation between ^{11}C-PiB and ^{124}I-mAb158-scFv8D3 in ArcSwe animals. Values display the Pearson correlation coefficient (R). *:P < 0.05, **: P < 0.01, ***: P < 0.001, ****: P<0.0001. (Ctx=cortex, Cer=cerebellum, Hpc=hippocampus, Thl=thalamus)

	^{124}I-mAb158-scFv8D3 Ctx	^{124}I-mAb158-scFv8D3 Cer	^{124}I-mAb158-scFv8D3 Hpc	^{124}I-mAb158-scFv8D3 Thl
^{11}C-PiB Thl				0.35 *
^{11}C-PiB Hipp			0.35 *	
^{11}C-PiB Cer		0.21 *		
^{11}C-PiB Ctx	0.34 *			

Supplementary Table 5. Correlation between ^{11}C-PiB and ^{125}I-mAb158-scFv8D3 in *App*$^{NL-G-F}$ animals. Values display the Pearson coefficient (R). *:P < 0.05, **: P < 0.01, ***: P < 0.001, ****: P<0.0001. (Ctx=cortex, Cer=cerebellum, Hpc=hippocampus, Thl=thalamus)

	^{125}I-mAb158-scFv8D3 Ctx	^{125}I-mAb158-scFv8D3 Cer	^{125}I-mAb158-scFv8D3 Hpc	^{125}I-mAb158-scFv8D3 Thl
^{11}C-PiB Thl				-0.19
^{11}C-PiB Hipp			-0.15	
^{11}C-PiB Cer		0.039		
^{11}C-PiB Ctx	-0.21			